Journal of
Materials Chemistry B

Materials for biology and medicine

Accepted Manuscript

This article can be cited before page numbers have been issued, to do this please use: S. Sang, X. Guo, J. Wang, H. Li and X. Ma, *J. Mater. Chem. B*, 2020, DOI: 10.1039/D0TB00354A.

ROYAL SOCIETY OF CHEMISTRY

rsc.li/materials-b

View Article Online
DOI: 10.1039/D0TB00354A

ARTICLE

Real-time and label-free detection of *VKORC1* gene based on a magnetoelastic biosensor for warfarin therapy

Received 00th January 20xx,
Accepted 00th January 20xx

DOI: 10.1039/x0xx00000x

Shengbo Sang[a†], Xing Guo[a†], Jingzhe Wang[a], Hongmei Li[a], Xingyi Ma[*a,b,c]

Various thrombotic disorders have been treated with the anticoagulant warfarin. However, a small change in warfarin concentration may lead to drug adverse reactions or therapeutic failure due to its narrow therapeutic index. Therefore, the dose of warfarin must be monitored for each patient during therapy in the real-time, sensitive and stable manner. In this work, we designed a magnetoelastic (ME) biosensor using Metglas alloy 2826 to detect VKORC1 genotype, which is one of the most important known genetic determinants of warfarin dosing. The sensor enabled both fast responses to DNA binding and wireless transmission of signals. Especially in the target recognition layer, the sensor introduced an avidin-biotin interaction system for signal amplification by increasing the surface load mass. The resonance frequency shift of the signal was linear to the concentration of the target in the range of 0.1 fM to 10 pM, with the detection limit (LOD) of 0.00389 fM (S/N = 3) and the sensitivity of 45.7 Hz/pM. Importantly, this ME-based biosensor was small and portable without the use of any optical labels, which has high potential to be applied in advanced biomedical diagnosis of nucleic acids and proteins.

Introduction

Warfarin is the most widely used anticoagulant for the treatment of stroke, deep vein thrombosis, pulmonary embolism and severe coronary thromboembolic diseases[1-3]. However, warfarin has a quite narrow therapeutic index and thus a small change in warfarin concentration may lead to drug adverse reactions or therapeutic failure [4-6]. Therefore, it is necessary to accurately adjust the dosage of warfarin for individual differences[7]. The drug differentiation factor of the individual is determined by the genotype of the drug-metabolizing enzyme that targets to warfarin[8]. Vitamin K epoxide reductase complex subunit 1 (VKORC1) is the primary molecular target of warfarin, and the *VKORC1* polymorphism has a great influence on the dosage of warfarin, of which the -1639G>A polymorphism has been demonstrated as a major marker for predicting the efficacy of warfarin[9].

Single nucleotide polymorphism is the most difficult genetic alteration to detect due to their subtle nature[10, 11]. In fact, recent studies have shown that single point mutations only moderately impact the global duplex structure[12]. Biomedical diagnosis of point mutations, G>A polymorphism in especial, suffers from the difficulty in identification of week variation of double stranded DNA[13]. Mismatched bases engage in promiscuous dynamic hydrogen bonding on a nanosecond time scale. This so-called breathing of bases generates significant changes in base orientation around glycosidic bonds, leading to abnormal binding affinity between the two nucleic acid strands. Unfortunately, G>A is the least-recognized purine-purine mutation because of its low breathing frequency[14]. Up to date, the detection of the *VKORC1* mutant gene has mainly relied on polymerase chain reaction (PCR) and sequencing, by which mutations are analyzed after the target sequence has been amplified by PCR[15]. The available methods including sequencing, gel mobility shift assay, and filter/chip binding assays are labor-intensive and consumes large amounts of reagent[16-19], which additionally require the labeling of probes and hence introduce artifacts; moreover, such methods need DNA samples at a high concentration at the level of 10~15 fmol for visualization, and thus have low resolution and sensitivity. It is of great significance to develop a direct and highly sensitive method for the detection of *VKORC1* gene in biomedicine[20-22].

In various sensor applications, Metglas alloy 2826 ($Fe_{40}Ni_{38}Mo_4B_{18}$), as amorphous alloy metal glass, has been successfully commercialized that detect change in resonant frequency as a result of stress applied to the sensor. The magnetoelastic (ME) materials based on amorphous Fe alloy have unique properties[23, 24]. The ME material has magnetostrictive effect and reversible changes due to changes in external magnetic field conditions. The ME material effectively converts the magnetic energy into mechanical vibrations when it is subjected to the alternating magnetic field generated by the coil[25]. It has fast mechanical response, high power density, and high coupling coefficient[26]. Biosensors have highlighted the uses of ME materials in terms of the high controllability, high production yield and low cost.[27-29] The ME materials show high potential in portable point-of-care (POC) biomedical applications and easy-to-operate mobile health owing to the following reasons. First, the ME material can achieve wireless detection, without need of electrical connection between the material and the monitoring system. Further, it is passive, without need of internal power. The capability of wireless sensing and driving in magnetic fields makes the ME material superior to the other

[a.] *MicroNano System Research Center, College of Information and Computer & Key Laboratory of Advanced Transducers and Intelligent Control System of Ministry of Education and Shanxi Province, Taiyuan University of Technology, Taiyuan, 030024, China.*
[b.] *Division of Intelligent Bio-systems, Korea Blockchain Institute, Seocho, Seoul 06651,Republic of Korea.*
[c.] *Jiangsu Shenhua Pharmaceutical Co., Jinhu 211600, China.*
† These authors contributed equally to this work.
*Corresponding author: maxy@korea.ac.kr.

materials for biomedical sensors[30]. In addition, ME materials response to biological interactions in the dye (label)-free and real-time manner.

The ME material is placed in a copper coiled glass tube, generating mechanical vibrations under the excitation by the network vector. When the mechanical vibration of the material matches with the vibration of the applied magnetic field as resonance, the conversion of electrical energy to elastic energy is maximized. For an ME chip, the fundamental resonant frequency of the base surface vibration is given by the equation (1) [31]:

$$f = \sqrt{\frac{E}{\rho(1-\sigma^2)}}\frac{1}{2L} \qquad (1)$$

where E represents the Young's modulus of elasticity, ρ is the density, σ is the Poisson's ratio, and L is the length of the ME chip. When the probe molecules modified on the surface of the ME chip specifically capture the targets, the surface quality changes and leads to the change of the resonance frequency of the ME surface, as shown in the equation (2) [32]:

$$\Delta f = -\frac{f}{2}\cdot\frac{\Delta m}{M} \qquad (2)$$

where f is the initial resonant frequency, M is the initial mass of the ME chip, Δm is the mass change (far less than M), and Δf is the displacement frequency. Based on the unique magnetostrictive characteristics, the biological information can be converted into measurable frequency signals.

In spite of the considerable advantages, there are still some limitations for the application of Metglas alloy 2826 in biomedicine. Fe-based alloys have poor corrosion resistance and biocompatibility. On the other hand, the sensing mechanism is based on the quality changes on the ME material surface. However, the DNA mass is relatively small[33], the sensing process based on the quality change of the chip requires a high stable platform better with strong signal amplification. Here we designed a protective layer of chromium to improve the corrosion resistance and a gold layer to improve the biocompatibility on the biosensor[21, 34], and we introduced a biotin-avidin interaction system to amplify the signal and enhance the sensitivity. The biotins of small size (molecular weight, 244.31 g/mol) modified on the end of DNA did not induce steric hindrance or occupy the reaction sites. They interacted with avidins with very high affinity (K_a, 1×10^{-15} M) [35]. The biotin-avidin system was resistant to extreme temperature, pH, organic solvents and common denaturation agents[36]. Importantly, avidins with the molecular weight of 66 kD increased the surface mass variation and amplified signals greatly. We also firstly demonstrated the ME-based biosensor to wirelessly detect *VKORC1* gene for guiding rational clinical therapy with warfarin (Fig. 1). Specifically, the thiolated capture probes (CP) were covalently immobilized on the surface of the gold-plated Metglas alloy 2826 to form the first specific recognition layer towards the target DNA molecules (tDNA). The 6-Mercapto-1-hexanol (MCH) was used to remove free CP from the surface. After the recognition of tDNA by the CP, the biotinylated DNA (biotin-DNA) further specifically hybridized with tDNA to form a sandwich structure. Finally, the big molecule avidin was introduced in the platform, leading to an increase in the surface load mass through the specific binding with biotin, and thus a decrease in the resonance frequency. This design of the sensing platform was proved to be effective and sensitive, where avidin acted as a direct signal indicator for the label-free and real-time detections of *VKORC1*.

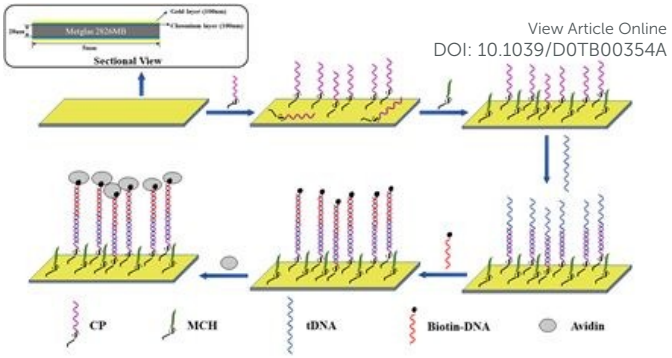

Fig. 1 Scheme of the ME-based biosensor platform.

Experimental

Reagents and materials

The ME material (Metglas alloy 2826) was offered by Honeywell, USA. Ethylenediamine tetraacetic acid (EDTA), tris(2-carboxyethyl)phosphine (TCEP) and MCH were purchased from Sinopharm Group, Shanxi, China. Avidin and tris-(hydroxymethyl) aminomethane were provided by Sangon Biotech. Co., Ltd, Shanghai, China. Phosphate bufered saline (PBS bufer, pH = 7.4), N-hydroxysuccimide (NHS), and N-ethyl-N%-(3-(dimethyl)aminopropyl)carbodiimide hydrochloride (EDC) were purchased from Sigma-Aldrich Corporation, Saint Louis, USA. The synthesis and modification of the oligonucleotides were accomplished by Sangon Biotech. Co., Ltd. The sequence information was shown in Table 1.

Table 1 Oligonucleotides used in this work.

DNA Name	DNA Sequence
CP	5'-GTTGAGGGCTTAGTGTTTTT-SH-3'
tDNA	5'-CACTAAGCCCTCAACCCAAGCCAGGCTGAC-3'
Biotin-DNA	5'-Biotin-TTGTCAGCCTGGCTTGG-3'
Single-base mismatched sequence (Mis-1-1)	5'-CACTCAGCCCTCAACCCAAGCCAGGCTGAC-3'
Single-base mismatched sequence (Mis-1-2)	5'-CACTAAGCCCTCAACCCAAGCCAGGGTGAC-3'
Two-base mismatched DNA (Mis-2)	5'-CACTCAGCCCTCAACCCAAGCCAGGGTGAC-3'
Non-complementary DNA (N-DNA)	5'- CTACGTAACCTGGCTAAGCCTAAGGCATGC-3'

Instruments

ME materials were cut by HP-603 precision automatic scribing machine (Shenzhen Kaixuan Industry Co., LTD). The resonant frequency measurement was performed on a vector network analyzer (AV3620A, Agilent, USA). The energy-dispersive spectroscopy (EDS) was operated by SU3500 (Hitachi, Japan) at an accelerate voltage of 15 kV. Images of the atomic force microscope (AFM) were obtained using NX10 atomic force microscope (Park Systems).

Fabrication of the biochip

The Metglas alloy 2826 was cut into chips of 5 mm ×1 mm × 0.028 mm rectangle using a cutting machine. Then the chips were sonically cleaned in acetone and ethanol for 15 min to remove residual debris, and dried in nitrogen stream. On the surfaces of the chip, a layer of metallic chromium with a thickness of about 100 nm covered by plasma sputtering, which was used both as an adhesive layer and a protective layer for the substrate material rich in iron. Another layer of gold of 100-nm thickness was coated on the surface of the chromium. The gold provided a bioactive attachment layer for the biomolecules. Then the chips were annealed in a 200°C vacuum furnace for 3 h to eliminate the residual organics and improve the stability of the prepared layers.

The above prepared substrate was ultrasonic cleaned with acetone, isopropanol, deionized water, and anhydrous ethanol for 5 min respectively, and then dried with nitrogen. Then it was immersed in the CP buffer solution with a concentration of 5 μM for 12 h. The buffers used in this study were shown in Table 2. Note that the buffering environment was important for the DNA detection[37]. TCEP was an efficient disulfide bond reducing agent to maintain the free sulfhydryl group in CP. After taking out from CP solution, the substrate was washed with deionized water, followed by immersing inside MCH solution to remove any non-specific adsorption of CP, rinsing with deionized water and blowing with nitrogen. The tDNA was diluted to be 10 pM, 1 pM, 100 fM, 10 fM, 1 fM, and 0.1 fM, respectively, and introduced on the as-prepared substrate at 37℃ for 1 h to hybridize with CP. The chip was cleaned with water and nitrogen before immersed in biotin-DNA (100 μM) solution that was complementary to the tDNA at 37℃ for 1 h. Then it was washed with Tris-HCl buffer (pH 7.4) and dried with nitrogen. Finally, the chip was equipped for the subsequent detection.

Detection of targets

NHS (40 mM) and EDC (20 mM) solutions were added to the avidin solution at the concentration of 100 μM for a 30-min activation at room temperature for subsequent testing. In the detection step, the combination of avidins and biotin caused a change in the signal, which was detected by the network vector analyzer. The enameled wire with a diameter of 0.202 mm was wound around the glass tube with a diameter of 8 mm to make the coil, which can convert the AC signal from the network vector analyzer into an alternating magnetic field. Resonance occurred when the vibration frequency of the chip was consistent with the alternating magnetic field. At the point, the conversion was the largest and the output signal value was the smallest, termed as S11 point. To increase the vibration amplitude of the ME material, a bar magnet was used to provide a DC offset magnetic field. The S11 point changed when the mass change occurred on the chip. The chip was vertically and wirelessly inserted in the glass tube containing the activated avidin solution. As the ME sensor is magnetostrictive, the resonance vibrations were actuated through magnetic fields. It is worth mentioning that the output signals were measured by the coil wirelessly, without a connection between the chip and the detection system.

Table 2 Buffers used in this work.

Molecule Name	Buffer	pH
CP	10 mM Tris-HCl, 1.0 mM EDTA, 1.0 mM TCEP	7.4
tDNA	10 mM Tris-HCl, 1.0 mM EDTA	7.4
Biotin-DNA	PBS buffer	7.4
Avidin	Ultrapure water	7.0

Results and discussion

Characterization of the chip

EDS was used to analyze the surface components during the fabrication and detection processes of the chip. The EDS images were shown in Fig. 2. The first column was the bare chip surface as control. Among all the elements, N and P were from DNA only. The surface element distribution mapping of MCH/CP/ME indicated the successful modification of CP on the surface as shown in the images of the first column. The N and P elements were evenly distributed with a high surface coverage, indicating that the DNA strands of the CP exhibited electrostatic repulsion with steric effect. The strands assembled into comb type while the MCH removed the excess and crosslinked CP on the surface. When tDNA was induced, the densities of the elements increased remarkably, indicating the capture of tDNA by the chip. Note that the EDS mapping was conducted after at least 3-times wash and blow with deionized water and nitrogen sequentially. The same results were confirmed for the hybridization of biotin-DNA. In the step of detection, as shown in the last column, the element densities were significantly increased, which was generated by the avidin of large molecular weight.

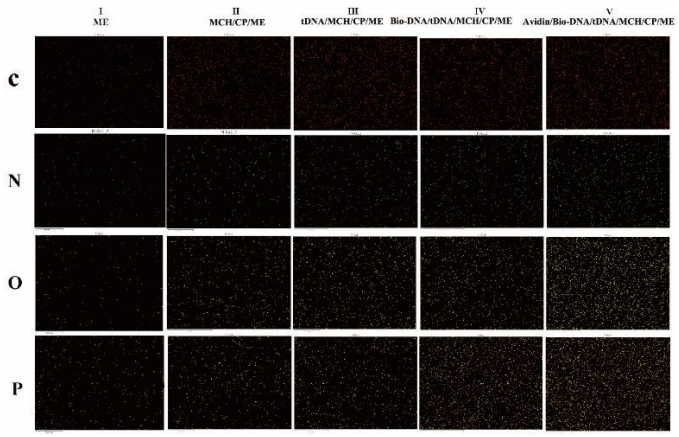

Fig. 2 The EDS images of the chip surface during modification and detection processes.

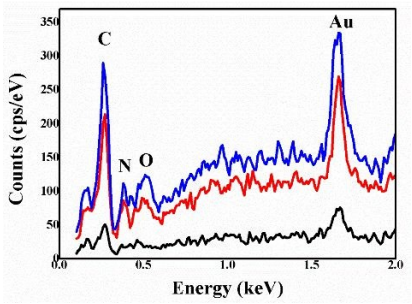

Fig. 3 Elemental analysis of the chip surface.

Furthermore, the EDS spectrums for elemental analysis of the chip surface were obtained as shown in Fig. 3. The black line showed the element content of the bare ME surface while the red line showed that of biotin-DNA/tDNA/MCH/CP/ME. The contents of the elements C, N and O increased significantly as marked in the figure. The introduction of avidin further enhanced the element content as shown in the blue line. EDS analysis proved the feasibility of the design of the ME-based DNA chip.

AFM was used to observe the three-dimensional topography of the chip surface after every step of sensing, as shown in Fig. 4. The surface of the gold coating layer was shown in Fig. 4A. The surface roughness was 4.260 nm with protrusions of the uniform gold nanostructure. After CP and MCH were conjugated on the chip surface by Au-S bond as shown in Fig. 4B, the surface height increased and the roughness increased to 6.539 nm. Interestingly, the capture of the tDNA decreased the surface roughness to be 4.684 nm (Fig. 4C). This may result from the formation of double stranded DNA of CP with the tDNA, which has much higher persistence length (~50 nm) than the single stranded DNA. This was proved again by the following hybridization of biotin-DNA with tDNA, forming a full double stranded helix and resulting into a further decrease of the roughness to be 3.803 nm. The topography of the chip surface after the detection step was shown in Fig. 4E. The height clearly increased with a surface roughness of 18.458 nm. The AFM topography indicated that the chip effectively captured target VKORC1 DNA with a successful secondary binding of avidins in the sandwich structure.

Sensing performance of the chip

Under the same experiment conditions, the resonance frequency responses of the chip to different concentrations of tDNA were detected, as shown in Fig. 5. After the specific binding of biotin and avidin, the surface mass increased and the resonance frequency

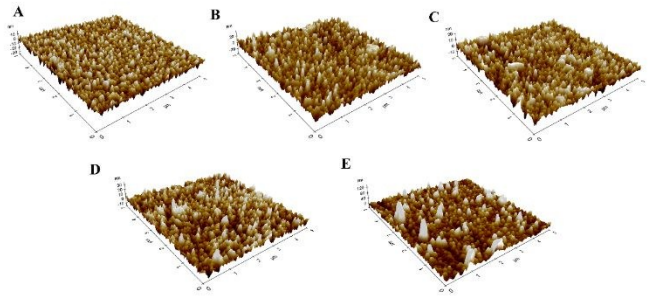

Fig. 4 AFM images of the chip in each step of biosensor fabrication for (A) gold layer coating; (B) probing layer modification; (C) tDNA capturing; (D) biotin-DNA hybridization and (E) Avidin amplification.

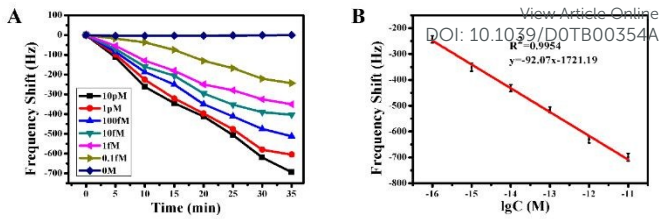

Fig. 5 (A) Real-time responses to tDNA of different concentrations. (B) Calibration curve of frequency shift versus the logarithmic tDNA concentration values.

decreased, reaching a stable state in about 35 minutes. As shown in the dark blue line of Fig. 5A, the higher the tDNA concentration, the greater the shift of the resonance frequency. In order to verify that the shift in resonance frequency was due to the specific reaction between biotin and avidin, tDNA of 0M was measured as control. There was no significant shift in the resonance frequency, demonstrating that non-specific adsorption could be ignored.

Fig. 5B shows the calibration curve of frequency shift versus the logarithmic tDNA concentration by three parallel experiments for each sample. There was a linear relationship between the frequency response of the chip and the concentration from 0.1 fM to 10 pM with the sensitivity of 45.7 Hz/pM. The fitted regression equation was $\Delta f = -92.07 \log C - 1721.19$ ($R2 = 0.9954$). The limit of detection (LOD) was calculated to be 0.00389 fM (S/N = 3), and a very low limit of quantification (LOQ) was achieve as 0.1 fM. The experimental results showed that the chip for the tDNA detection has a high sensitivity and good linear response.

Specificity, stability and reproducibility of the chip

In order to check the specificity of the chip, the frequency response of the chip to target with a single base substitution was detected, as shown in Fig. 6A. The Mis-1-1 was the target that had a single base mismatching with the CP, and the Mis-1-2 had a single base mismatching with the biotin-DNA. The Mis-2 was the target that had two single base mismatching with the CP and biotin-DNA, respectively. The mismatches were marked in yellow in Table 1. The results proved that the chip could distinguish point mutations in both the probing part and the biotin-avidin amplification part of the sandwich structure, showing high specificity. Similarly, a random sequence (N-DNA) did not produce any frequency shift of signals.

The stability of chip was investigated by detecting the frequency response of seven chips for 7 days. The seven chips modified with 100 fM tDNA were prepared at the same time under the same conditions, and their frequency response to avidin was tested every day, as shown in Fig. 6B. The change of the resonance frequency within 7 days was consistent, and the relative standard deviation (RSD) was 2.1%,

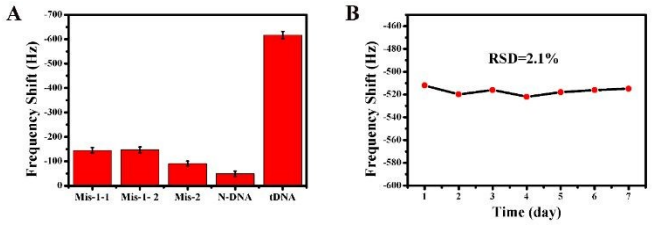

Fig. 6 (A) Real-time response of the chip to different targets. (B) Investigation of the sensing stability by measurements of 100 fM tDNA for 7 days.

indicating an excellent stability of the chips. In addition, the frequency response of three chips prepared under the same conditions to 1 fM tDNA was tested to evaluate the repeatability of chip, and the RSD of 9.81% was obtained, indicating the good reproducibility of this biosensor.

Conclusions

ME-based biosensor was fabricated to detect the VKORC1 gene using Metglas alloy 2826. The biocompatibility of the ME material was improved with gold layers of 100 nm in the thickness. The sandwich structure on the chip surface with three layers of CP, tDNA and biotin ensured the high sensitivity and specificity of the sensor. And the signal amplification by avidin realized the label-free detections of single nucleotide polymorphism in *VKORC1*. The sensor achieved the LOD of 0.00389 fM (S/N = 3) and the sensitivity of 45.7 Hz/pM. The signal of this sensor had a linear relationship with the target DNA concentration in the range of 0.1 fM to 10 pM. Importantly, the chip was portable for the entire operation, label-free for signal generation, wireless for signal readout, stable and reproducible for warfarin therapy in biomedicine.

Conflicts of interest

There are no conflicts of interest to declare.

Acknowledgements

The authors are grateful for the financial support from the National Natural Science Foundation of China (grant numbers 51975400, 61501316, 51505324). X. Ma acknowledges the grant from Korea Blockchain Institute (W2018B753) and China Postdoctoral Science Foundation (2017M621664).

References

1. T. Aomori, K. Yamamoto, A. Oguchi-Katayama, Y. Kawai, T. Ishidao, Y. Mitani, Y. Kogo, A. Lezhava, Y. Fujita, K. Obayashi, K. Nakamura, H. Kohnke, M. Wadelius, L. Ekstrom, C. Skogastierna, A. Rane, M. Kurabayashi, M. Murakami, P. E. Cizdziel, Y. Hayashizaki and R. Horiuchi, *Clin Chem*, 2009, **55**, 804-812.
2. N. B. Polito, E. Kanouse, C. M. C. Jones, M. McCann, M. A. Refaai and N. M. Acquisto, *Transfusion*, 2019, **59**, 1202-1208.
3. Y. Zhu, K. M. Swanson, R. L. Rojas, Z. Wang, J. L. St Sauver, S. L. Visscher, L. J. Prokop, S. J. Bielinski, L. Wang, R. Weinshilboum and B. J. Borah, *Genetics in medicine*, 2020, **22**, 475-486.
4. C. R. King, R. M. Porche-Sorbet, B. F. Gage, P. M. Ridker, Y. Renaud, M. S. Phillips and C. Eby, *Am J Clin Pathol*, 2008, **129**, 876-883.
5. A. Kwon, S. H. Jo, H. J. Im, Y. A. Jo, J. Y. Park, H. J. Kang, H. S. Kim, H. C. Cho and Y. K. Lee, *J Thromb Thrombolysis*, 2011, **32**, 467-473.
6. P. R. Vuddanda, M. Alomari, C. C. Dodoo, S. J. Trenfield, S. Velaga, A. W. Basit and S. Gaisford, *Eur J Pharm Sci*, 2018, **117**, 80-87.
7. R. R. Shah, *Journal of clinical pharmacy and therapeutics*, 2020.
8. S. A. Scott, L. Edelmann, R. Kornreich and R. J. Desnick, *Am J Hum Genet*, 2008, **82**, 495-500.
9. C.-Y. C. Tao Li, Da-Yun Jin, Pen-Jen Lin,Anastasia Khvorova & Darrel W. Stafford, *Nature*, 2004, **427**, 541-544.
10. M. Yasmin, G. Refregier, R. T. Siddiqui, R. Iqbal, S. A. Abbasi and S. Tahseen, *Tuberculosis (Edinb)*, 2018, **110**, 52-55.
11. A. Lázaro, E. S. Yamanaka, Á. Maquieira and L. A. Tortajada-Genaro, *Sensors and Actuators B: Chemical*, 2019, **298**, 126877.
12. X. Ma, S. Song, S. Kim, M. S. Kwon, H. Lee, W. Park and S. J. Sim, *Nat Commun*, 2019, **10**, 836.
13. G. Rossetti, P. D. Dans, I. Gomez-Pinto, I. Ivani, C. Gonzalez and M. Orozco, *Nucleic Acids Res.*, 2015, **43**, 4309-4321.
14. X. Zhou, D. Kondhare, P. Leonard and F. Seela, *Chemistry*, 2019, **25**, 10408-10419.
15. N. K. a. N. H. Takashi Tamura, *Methodology*, 2014, **3**, 499.
16. G. Daras, A. Alatzas, D. Tsitsekian, D. Templalexis, S. Rigas and P. Hatzopoulos, *Electrophoresis*, 2019, **40**, 1365-1371.
17. G. Sagner, R. Rüger and C. Kessler, *Gene*, 1991, **97**, 119-123.
18. Y. Liu, N. Lyu, V. K. Rajendran, J. A. Piper, A. Rodger and Y. Wang, *Anal. Chem.*, 2020.
19. W. Xu, T. Jin, Y. Dai and C. C. Liu, *Biosens. Bioelectron.* , 2020, **155**, 112100.
20. X. Ma, P. L. Truong, N. H. Anh and S. J. Sim, *Biosens. Bioelectron.*, 2015, **67**, 59-65.
21. Y. Zhang, M. Li, X. Gao, Y. Chen and T. Liu, *J Hematol Oncol*, 2019, **12**, 137.
22. F. Makiyan, F. Rahimi, M. Hajati, A. Shafiekhani, A. H. Rezayan and N. Ansari-Pour, *Colloids and surfaces. B, Biointerfaces*, 2019, **181**, 714-720.
23. S. Huang, H. Yang, R. S. Lakshmanan, M. L. Johnson, J. Wan, I. H. Chen, H. C. Wikle, 3rd, V. A. Petrenko, J. M. Barbaree and B. A. Chin, *Biosens Bioelectron*, 2009, **24**, 1730-1736.
24. L. Fu, K. Zhang, S. Li, Y. Wang, T.-S. Huang, A. Zhang and Z. Y. Cheng, *Sensors and Actuators B: Chemical*, 2010, **150**, 220-225.
25. C. A. G. Plamen G. Stoyanov, *Sensors and Actuators B: Chemical*, 2000, **80**, 8--14.
26. Sang S, Li Y, Guo X, Zhang B, Xue X, Zhuo K, Zhao C, Zhang W and Y. Z., *Biosens. Bioelectron.* , 2019, **141**, 111399.
27. J. Wang, X. Guo, R. Liu, J. Guo, Y. Zhang, W. Zhang and S. Sang, *Nanotechnology*, 2019, **31**, 015501.
28. S. Horikawa, D. Bedi, S. Li, W. Shen, S. Huang, I. H. Chen, Y. Chai, M. L. Auad, M. J. Bozack, J. M. Barbaree, V. A. Petrenko and B. A. Chin, *Biosens. Bioelectron.* , 2011, **26**, 2361-2367.
29. R. Guntupalli, J. Hu, R. S. Lakshmanan, T. S. Huang, J. M. Barbaree and B. A. Chin, *Biosens. Bioelectron.*, 2007, **22**, 1474-1479.
30. I. H. Chen, Y. Liu, S. Du, J. Hu, F. Wang, S. Horikawa, T.-S. Huang and B. A. Chin, *Advances in Microbiology*, 2019, **09**, 541-555.
31. N. Hiremath, R. Guntupalli, V. Vodyanoy, B. A. Chin and M.-K. Park, *Sensors and Actuators B: Chemical*, 2015, **210**, 129-136.
32. J. I. A. Rashid and N. A. Yusof, *Sensing and Bio-Sensing Research*, 2017, **16**, 19-31.
33. X. Ma and S. J. Sim, *Analyst*, 2013, **138**, 1794-1802.
34. X. Ma, J. Huh, W. Park, L. P. Lee, Y. J. Kwon and S. J. Sim, *Nat Commun*, 2016, **7**, 12873.
35. A. M. i. M.I. Pividori, S. Alegret, *Biosensors & Bioelectronics*, 2000, **15**, 291–303.
36. C. Zhang, Y. Li, M. Zhang and X. Li, *Tetrahedron*, 2012, **68**, 5152-5156.
37. S. R. Yan, M. M. Foroughi, M. Safaei, S. Jahani, N. Ebrahimpoor, F. Borhani, N. R. Z. Baravati, Z. Aramesh-Boroujeni and L. K. Foong, *Int. J. Biol. Macromol.*, 2020, **155**, 184-207.

The Table of Contents

View Article Online
DOI: 10.1039/D0TB00354A

This work designs the magnetoelastic biosensor to detect *VKORC1* gene for warfarin therapy in a fast, label-free and sensitive manner.